Dental Materials Journal 2017; 36(5): 573–583

Dose effects of beta-tricalcium phosphate nanoparticles on biocompatibility and bone conductive ability of three-dimensional collagen scaffolds

Shusuke MURAKAMI[1], Hirofumi MIYAJI[1], Erika NISHIDA[1], Kohei KAWAMOTO[1], Saori MIYATA[1], Hiroko TAKITA[2], Tsukasa AKASAKA[3], Bunshi FUGETSU[4], Toshihiko IWANAGA[5], Hiromi HONGO[6], Norio AMIZUKA[6], Tsutomu SUGAYA[1] and Masamitsu KAWANAMI[1]

[1] *Department of Periodontology and Endodontology, Hokkaido University Graduate School of Dental Medicine, N13 W7 Kita-ku, Sapporo 060-8586, Japan*
[2] *Support Section for Education and Research, Hokkaido University Graduate School of Dental Medicine, N13 W7 Kita-ku, Sapporo 060-8586, Japan*
[3] *Department of Dental Materials and Engineering, Hokkaido University Graduate School of Dental Medicine, N13 W7 Kita-ku, Sapporo 060-8586, Japan*
[4] *Nano-Agri Lab, Policy Alternatives Research Institute, The University of Tokyo, 7-3-1, Tokyo 113-0033, Japan*
[5] *Laboratory of Histology and Cytology, Hokkaido University Graduate School of Medicine, N15 W7 Kita-ku, Sapporo 060-8638, Japan*
[6] *Department of Developmental Biology of Hard Tissue, Hokkaido University Graduate School of Dental Medicine, N13 W7 Kita-ku, Sapporo 060-8586, Japan*
Corresponding author, Hirofumi MIYAJI; E-mail: miyaji@den.hokudai.ac.jp

Three-dimensional collagen scaffolds coated with beta-tricalcium phosphate (β-TCP) nanoparticles reportedly exhibit good bioactivity and biodegradability. Dose effects of β-TCP nanoparticles on biocompatibility and bone forming ability were then examined. Collagen scaffold was applied with 1, 5, 10, and 25 wt% β-TCP nanoparticle dispersion and designated TCP1, TCP5, TCP10, and TCP25, respectively. Compressive strength, calcium ion release and enzyme resistance of scaffolds with β-TCP nanoparticles applied increased with β-TCP dose. TCP5 showed excellent cell-ingrowth behavior in rat subcutaneous tissue. When TCP10 was applied, osteoblastic cell proliferation and rat cranial bone augmentation were greater than for any other scaffold. The bone area of TCP10 was 7.7-fold greater than that of non-treated scaffold. In contrast, TCP25 consistently exhibited adverse biological effects. These results suggest that the application dose of β-TCP nanoparticles affects the scaffold bioproperties; consequently, the bone conductive ability of TCP10 was remarkable.

Keywords: Biomaterial, Cell ingrowth, Nano-dispersion, Bone tissue engineering

INTRODUCTION

Bone tissue engineering aims to create new functional bone *via* synergistic therapy using three biological elements[1)] (cells[2-4)], signaling molecules[5-8)], and natural and artificial scaffolds[9-11)]) in order to reverse bone loss caused by infectious disease[12-15)], trauma[16)], and cancer[17)] or to augment host bone for dental implants[18,19)]. Application of a three-dimensional (3D) scaffold to the bone defect produces a regenerative space for tissue reconstruction and stimulates cell proliferation and differentiation, along with angiogenesis and extracellular matrix secretion[20)]. Therefore, refining the specifications of the regenerative scaffold is required for clinical up-regulation of bone structure and function.

Bioceramics such as calcium phosphate and hydroxyapatite (HA) are widely known as bio-safe materials and bone graft substitutes[21,22)]. Nano-modification of biomaterials *via* nanosized bioceramics might play a major role in promoting their properties for biomedical applications[23-26)]. Ibara *et al.* and Ogawa *et al.* prepared a 3D collagen scaffold with surface-modifications using beta-tricalcium phosphate (β-TCP) nanoparticles and subsequently implanted the scaffold in combination with fibroblast growth factor-2 (FGF-2) into rat connective tissue[27,28)]. They observed that the promotion of cell and tissue ingrowth into the scaffold was facilitated by β-TCP nanoparticle modification. Ogawa *et al.* also demonstrated that scaffolds loaded with β-TCP nanoparticles and FGF-2 accelerated reconstruction of periodontal organs, including alveolar bone, cementum, and periodontal ligament-like tissue, suggesting that scaffolds modified with β-TCP nanoparticles and FGF-2 can induce the formation of functional bone structures.

The applied dose of nanomaterial serves an important role in determining biocompatibility. Nanomaterials exhibit a high level of bioactivity. Therefore, adverse effects are expected to occur in biomedical applications. Huang *et al.* assessed the effects of applying HA nanoparticles (<100 nm) *in vitro*[29)]. A high dose of HA nanoparticles stimulated the attachment and growth of osteoblastic cells, but it also induced lactate dehydrogenase production in macrophages, suggesting that HA is cytotoxic. Furthermore, Nishida *et al.* and Schrand *et al.* reported that the use of nanocarbons with a high nanocarbon to substrate ratio in biomaterials was associated with reduced cell viability[30,31)]. Therefore, we hypothesized that application of β-TCP nanoparticles at different

Color figures can be viewed in the online issue, which is available at J-STAGE.
Received Aug 26, 2016: Accepted Dec 24, 2016
doi:10.4012/dmj.2016-295 JOI JST.JSTAGE/dmj/2016-295

content ratios would affect the biocompatibility and bone-forming ability of the 3D scaffold following implantation. This study was conducted to assess the dose effects of β-TCP nanoparticles on scaffold biological properties *in vitro* and *in vivo*. Additionally, we evaluated augmentation of rat cranial bone following implantation of scaffolds loaded with β-TCP nanoparticles at different doses.

MATERIALS AND METHODS

Fabrication and characterization of β-TCP nanoparticle-modified scaffolds

Dispersion of β-TCP nanoparticles was carried out as described previously[27]. β-TCP powder (Beta TCP; Tomita Pharmaceutical, Naruto, Japan) was pulverized into nano-sized particles using a pulverizer (Nanomizer, Yokohama, Japan). The peak profile of β-TCP powder *via* X-ray diffraction investigations was overlapped with the data of the previous report[27,32]. The β-TCP nanoparticles, along with the surfactant sodium cholate (0.2 wt%), were then dispersed in 1-methyl-2-pyrrolidone (Wako Pure Chemical Industries, Osaka, Japan). Four nano–β-TCP dispersion doses (1, 5, 10, and 25 wt%) were used for application. The mean particle size of the β-TCP nanoparticles was 85 nm, as revealed by particle size distribution analysis (LB-550; Horiba, Kyoto, Japan).

Each β-TCP dispersion (100 μL) was injected into a 3D collagen scaffold (Terudermis®, 6×6×3 mm^3; Olympus Terumo Biomaterials, Tokyo, Japan) using a syringe with a 25-gauge needle. Then the scaffold was immersed in ethanol to remove the dispersion solution. After several rinses in ethanol followed by air-drying, scaffolds were obtained for assessment and labeled respectively as TCP1, TCP5, TCP10, and TCP25 (Fig. 1A). Collagen scaffold without β-TCP nanoparticle modification was also assessed as a control and was labeled as COL.

Surface nanostructures and cut sections of the scaffold were characterized using scanning electron microscopy (SEM, S-4000; Hitachi, Tokyo, Japan) with an accelerating voltage of 10 kV after coating with a thin layer of Pt-Pd. Chemical distribution mapping and composition analysis of the scaffolds with β-TCP nanoparticle modification were carried out using energy-dispersive X-ray spectrometry (EDS, JSM-6500F, 15 kV; JEOL, Tokyo, Japan) after coating with a thin layer of carbon. Compression tests for each scaffold were conducted using a universal testing machine (EZ-S; Shimadzu, Kyoto, Japan). The cross-head loading speed was set at 0.5 mm/min. The scaffold porosity was calculated using the following equation:

$$\text{Porosity}=100\times(1-\rho1/\rho2),$$

where ρ1=the bulk density and ρ2=the theoretical density of the scaffold. The bulk densities were calculated from measurements of the volumes and weights of β-TCP and collagen, respectively. The theoretical density was obtained from previous studies[33,34]. Subsequently, each scaffold was subjected to *in vitro* enzymatic degradation testing. Pre-weighed dry specimens were immersed for 3 h at 37°C in phosphate-buffered saline (PBS) with 1% collagenase type I (0.1 mg/mL; Wako Pure Chemical Industries). After ethanol dehydration and air drying, the weight loss of the scaffold was determined. In addition, test of calcium ion release from the scaffolds were conducted. COL, TCP5, and TCP25 were immersed in PBS at 37°C. The calcium content after 7 days was measured in the supernatants using a calcium test kit (calciumE-test; Wako Pure Chemical Industries).

Cytocompatibility test

Mouse osteoblastic MC3T3-E1 cells (1×10^4; RIKEN BioResource Center, Tsukuba, Japan) were seeded onto the scaffolds and cultured in humidified 5% CO_2 at 37°C, using minimum essential medium (MEM) (alpha-GlutaMAX™-I; Thermo Fisher Scientific, Waltham, MA, USA) supplemented with 10% fetal bovine serum (FBS) (Qualified; Thermo Fisher Scientific) and 1% antibiotics (penicillin/streptomycin; Thermo Fisher Scientific). Cell viability was assessed after 1, 3, 5, and 7 days of culture using a WST-8 cell counting kit-8 (CCK-8; Dojindo Laboratories, Mashiki, Japan), in accordance with the manufacturer's instructions. The optical density was measured using a microplate reader at 450-nm absorbance. After 1 day of culture, some samples were fixed in 2.5% glutaraldehyde in 0.1 M sodium cacodylate buffer (pH 7.4) for 30 min and then rinsed in cacodylate

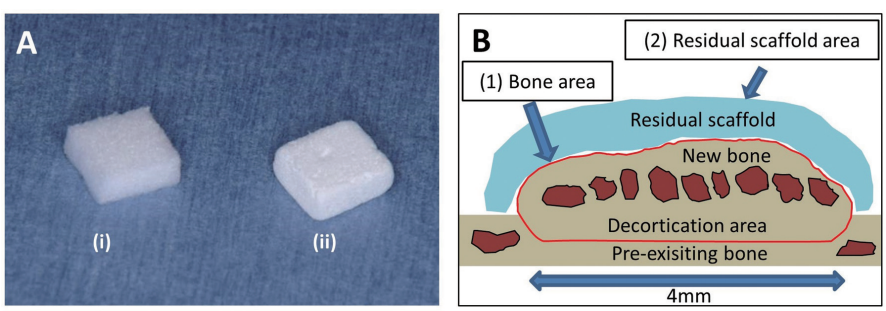

Fig. 1 (A) Digital photograph of COL (i) and TCP25 (ii). (B) Schematic drawing of histomorphometric analysis.
The frontal plane view indicating the following parameters: the area of newly formed bone (1) and the area of residual scaffold (2).

buffer solution. Some samples were then dehydrated in increasing concentrations of ethanol. Following critical point drying, samples were analyzed using SEM.

Assessment of rat subcutaneous tissue responses

Animal experimental protocols followed the institutional animal use and care regulations of Hokkaido University (Animal Research Committee of Hokkaido University, approval number 10–42). Ten-week-old male Wistar rats weighing 190–210 g were given general anesthesia by intraperitoneal injections of 0.6 mL/kg sodium pentobarbital (Somnopenthyl; Kyoritsu Seiyaku, Tokyo, Japan), as well as a local injection of 2% lidocaine hydrochloride with 1:80,000 epinephrine (Xylocaine Cartridge for Dental Use; Dentsply Sankin, Tokyo, Japan). After a skin incision was made in back of each rat, each scaffold was implanted into the subcutaneous tissue. Skin flaps were sutured (Softretch 4-0; GC, Tokyo, Japan), and tetracycline hydrochloride ointment (Achromycin Ointment; POLA Pharma, Tokyo, Japan) was applied to the wound. Rats were euthanized by administration of an overdose of sodium pentobarbital (2.0 mL/kg) at 10 days post-surgery.

For DNA measurement (n=6), some specimens extracted from the wound were freeze-dried. Following pulverization, 0.5 mL of 2 M NaCl and 0.05 M phosphate buffer (pH 7.4) were added to each scaffold. After centrifugation, the DNA content of the infiltrated cells was measured using a DNA quantification kit (Primary Cell, Sapporo, Japan) according to the manufacturer's instructions, using a fluorescence spectrophotometer (F-3000; Hitachi) equipped with a 356-nm excitation filter and a 458-nm emission filter.

For histologic measurements (n=6), tissue blocks, including the surrounding soft tissues, were fixed in 10% buffered formalin, embedded in paraffin wax, and cut into 5-μm sections. Sections were stained with hematoxylin-eosin (HE) and observed histologically using light microscopy. Histomorphometric measurements of the residual scaffold and tissue ingrowth areas were performed using ImageJ software (ver. 1.41; National Institutes of Health, Bethesda, MD, USA). In addition, three area units (120 μm^2 per unit) were selected using light microscopy. The foreign body multinucleate giant cells around the β-TCP granules and collagen scaffold fibers at the periphery of the scaffolds were counted for three stained sections: one from the center of the excised tissue sample, and one each from tissue 1 mm to either side of the center.

Five rats receiving COL, TCP5, and TCP25 implantation were perfused *via* the aorta with physiologic saline, followed by 4% formaldehyde in 0.1 M phosphate buffer, pH 7.4. Tissue blocks were pre-fixed using 10% buffered formalin and then dipped in 30% sucrose solution. The tissues were embedded in OCT compound (Sakura Finetek Japan, Tokyo, Japan) and frozen quickly in liquid nitrogen. Frozen 16-μm sections were mounted on poly-L-lysine-coated glass slides. After pretreatment with 0.3% Triton X-100 and normal donkey serum, the sections were incubated overnight with the following primary antibodies, alone or in mixtures as indicated in the data: mouse anti-CD68 (1:100 dilution; AbD Serotec, Kidlington, UK), rabbit anti-galectin3 (gal3) (1:300 dilution, sc-20157; Santa Cruz Biotechnology, Santa Cruz, CA, USA), mouse anti-prolyl-4-hydroxylase beta (P4HB) (1:1600 dilution, clone6-9H6; Acris Antibodies, San Diego, CA, USA), mouse anti-rat endothelial cell antigen-1 (RECA-1) (1:1000 dilution; AbD Serotec), and mouse anti-alpha-smooth muscle actin (ASMA) (1:1600 dilution, clone 1A4; Sigma-Aldrich, St. Louis, MO, USA). The sites of antigen-antibody reaction were detected by incubation with Cy3-labeled anti-mouse IgG (Jackson Immuno Research Laboratories, West Grove, PA, USA) or AlexaFluor 488-labeled anti-rabbit IgG (Invitrogen, Eugene, OR, USA). Nuclear staining was performed by short incubation with TOTO3 (Invitrogen). The stained sections were mounted using glycerin-PBS and then observed under a confocal laser scanning microscope (Fluoview; Olympus, Tokyo, Japan). The specificity of the immunoreactions within the sections was confirmed according to a conventional procedure. Sections incubated with normal mouse or rabbit serum instead of respective primary antibody were used as negative controls. Subsequently, for detection of granulocytes, some sections were incubated in 0.01 M Tris-HCl buffer (pH 7.6) containing 0.01% 3,3′-diaminobenzidine (DAB) and 0.001% H_2O_2. The stained sections were observed under light microscopy.

Bone-forming test

Forty-five 10-week-old male Wistar rats were given general anesthesia by intraperitoneal injections of sodium pentobarbital (0.6 mL/kg), as well as a local injection of 2% lidocaine hydrochloride with 1:80,000 epinephrine. After a skin incision was made in the scalp, a flap was made and decortication of a 4×4 mm area was performed in front of the coronal suture in the cranial bone using a rotating round bur under water irrigation. Subsequently, each scaffold was placed on the cranial bone with decortication. Skin flaps were sutured. Tetracycline hydrochloride ointment was then applied to the wound. Rats were euthanized using sodium pentobarbital (2.0 mL/kg). Specimens were collected from the wound 10 days (n=3) and 35 days (n=6) after surgery. The tissue blocks, including the cranial bone and surrounding soft tissue, were fixed in 10% buffered formalin, decalcified in 10% EDTA, embedded along the frontal plane in paraffin wax, and cut into 6-μm sections located every 300 μm. Sections were prepared and stained with HE and Masson's trichrome. In addition, some paraffin sections were examined for alkaline phosphatase (ALPase). After pretreatment with 0.3% H_2O_2 and 1% bovine serum albumin (BSA; Serologicals Proteins, Kankakee, IL, USA) in PBS, the sections were incubated with rabbit antiserum against rat tissue nonspecific ALPase (1:100 in dilution) generated by Oda *et al.*[35] for 2 h. After rinsing, the sections were incubated with horseradish peroxidase-conjugated

anti-rabbit IgG (Chemicon International, Temecula, CA, USA) for 1 h. For visualizing the immunoreaction, DAB tetrahydrochloride was used as a substrate. The stained sections were observed under light microscopy. Subsequently, three HE stained sections were taken for histomorphometric measurements from the midsection of the scaffold. Measurements of the areas of newly formed bone and residual scaffold were performed for each stained section after 35 days using a software package (Fig. 1B).

Statistical analysis

Data are presented as the mean and standard deviation. Differences between groups were analyzed using the Scheffé test. Results for which p was <0.05 were regarded as statistically significant. All statistical analyses were performed using SPSS software (IBM SPSS 11.0; SPSS Japan, Tokyo, Japan).

RESULTS

Characterization of β-TCP nanoparticle-modified scaffolds

The SEM images in Figs. 2A–J show the nano-fine structure of the scaffolds modified by β-TCP nano-dispersion. β-TCP nanoparticles attached well to the surface of collagen fibers of the scaffold, even in the central region of the collagen scaffold. In SEM images of TCP1 and TCP5, collagen fibers appear coated by a thin layer of dispersed β-TCP nanoparticles. TCP1 and TCP5 exhibited an interconnected structure similar to COL (Figs. 2A–F). In contrast, the collagen fibers were fully wrapped by a thick layer of aggregated β-TCP nanoparticles in TCP10 and TCP25. The inner space of the collagen scaffold was partly filled with aggregated β-TCP particles in TCP10 and TCP25 (Figs. 2G–J). The porosity of each scaffold was calculated as >90% (Table 1). However, TCP25 showed significantly lower porosity when compared to the other scaffolds. EDS analysis of the surface of scaffolds containing β-TCP nanoparticles showed the presence of oxygen, phosphorus, and calcium (Figs. 3A–E). The compression strength of TCP25 was enhanced strongly by application of β-TCP nanoparticles, approximately 2.5-fold greater than that of COL. The difference was statistically significant. In addition, the compression strengths of TCP5 and TCP10 were significantly greater (1.5-fold) when compared to COL (Fig. 4A). In degradation tests, application of β-TCP nanoparticles to the scaffolds increased their resistance to enzymatic degradation. The decrement in the content of TCP25 scaffold after collagenase degradation was less compared with the other scaffolds (Fig. 4B). Calcium ion release by the scaffold modified with β-TCP nanoparticles increased in a dose-dependent manner (Fig. 4C).

Cytocompatibility test

After MC3T3-E1 cell seeding, marked cell spreading was

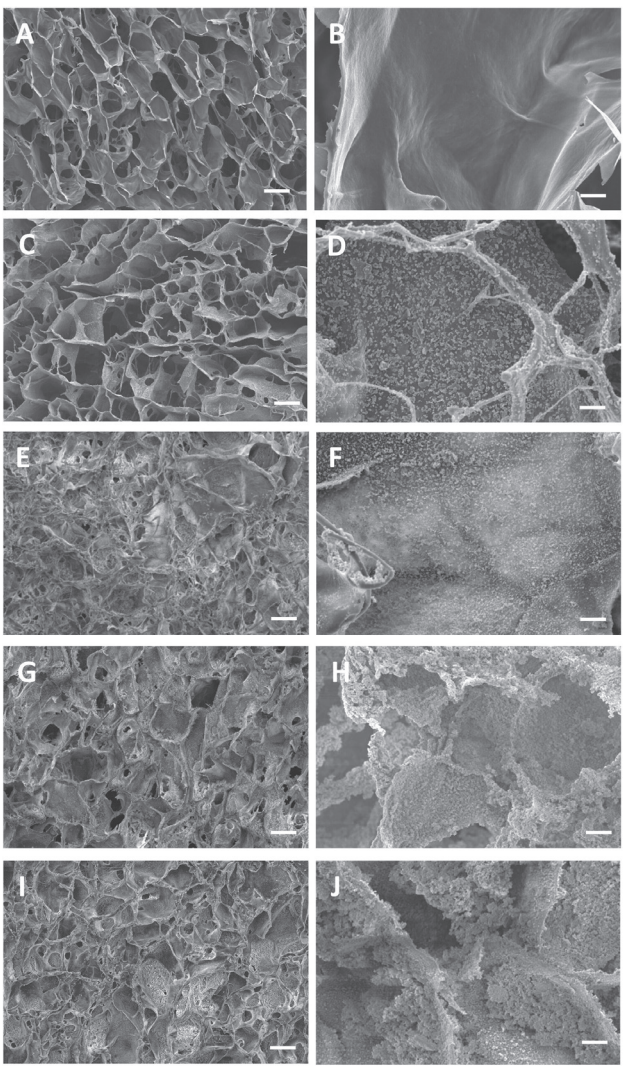

Fig. 2 SEM micrographs of COL (A,B), TCP1 (C, D), TCP5 (E, F), TCP10 (G, H) and TCP25 (I, J).
Scale bars respectively represent 10 μm (B, D, F, H, J) and 100 μm (A, C, E, G, I).

Table 1 Structural parameters of each scaffold (n=7, mean±SD)

	COL	TCP1	TCP5	TCP10	TCP25
β-TCP weight (mg)	—	1.0±0.2	3.6±0.5[b)]	10.4±1.4[bc)]	20.0±1.0[bcd)]
Porosity (%)	97.7±0.1	97.4±0.1	96.7±0.1[ab)]	94.9±0.3[abc)]	91.8±0.4[abcd)]

a, p< 0.05 *vs.* COL; b, p<0.05 *vs.* TCP1; c, p<0.05 *vs.* TCP5, d, p<0.05 *vs.* TCP10.

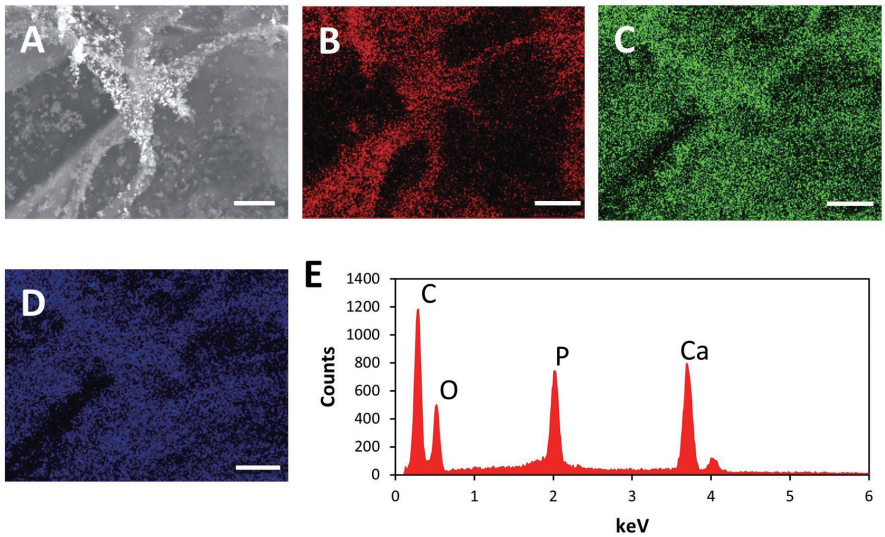

Fig. 3 Energy-dispersive X-ray spectrometry analysis of the surface of TCP5. SEM image (A), oxygen mapping (B), phosphorous mapping (C), calcium mapping (D), and EDS spectrum (E). Scale bars represent 10 μm.

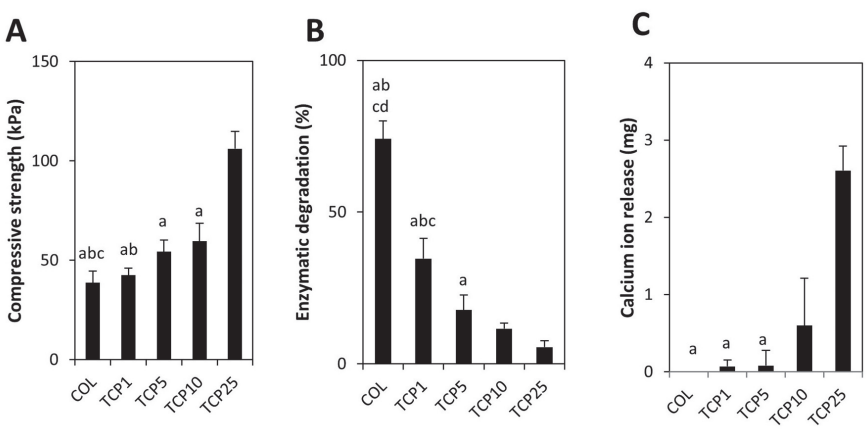

Fig. 4 Assessment of compressive strength (A), enzymatic degradation (B), and calcium ion release (C) for each scaffold (n=6, mean±SD).
a, p<0.05 *vs.* TCP25; b, p<0.05 *vs.* TCP10; c, p<0.05 *vs.* TCP5; d, p<0.05 *vs.* TCP1.

demonstrated on the surface of scaffolds modified with β-TCP nanoparticles (Figs. 5A–E). In the SEM image of TCP1 and TCP5, cell processes appear elongated on the nano-fine structure consisting of collagen fibers and β-TCP nanoparticles (Figs. 5B and C). Although the surface of the collagen scaffold was mostly covered with a thick layer of aggregated β-TCP nanoparticles in TCP10 and TCP25, cell attachment and spreading were also demonstrated (Figs. 5D and E). In assessment of cytocompatibility, MC3T3-E1 cell proliferation on TCP1, TCP5, and TCP10 was stimulated significantly by β-TCP nanoparticle application in a dose-dependent manner when compared with COL. Particularly, TCP10 exhibited prominent proliferation. Similarly, cell proliferation on TCP25 was greater than on COL, although TCP25 showed decreased cell proliferation compared with TCP10 (Fig. 5F).

Rat subcutaneous tissue responses

Greater cell ingrowth into the scaffold was observed in TCP1 and TCP5 when compared to COL (Figs. 6A–F). The tissue-ingrowth area of TCP5 was significantly greater (3.5-fold) compared with COL (Fig. 7A). Immunohistochemical analysis of TCP5 revealed that macrophages expressing CD68 and gal3 and fibroblasts expressing P4HB were frequently found in the scaffold

(Figs. 8B and E), suggesting that tissue remodeling occurred by scaffold degradation and subsequent production of extracellular matrix, such as collagen. In addition, TCP1 and TCP5 possessed tube-shaped blood-vessel-like structures as well as macrophage and fibroblast ingrowth (Figs. 6D and F). We also found

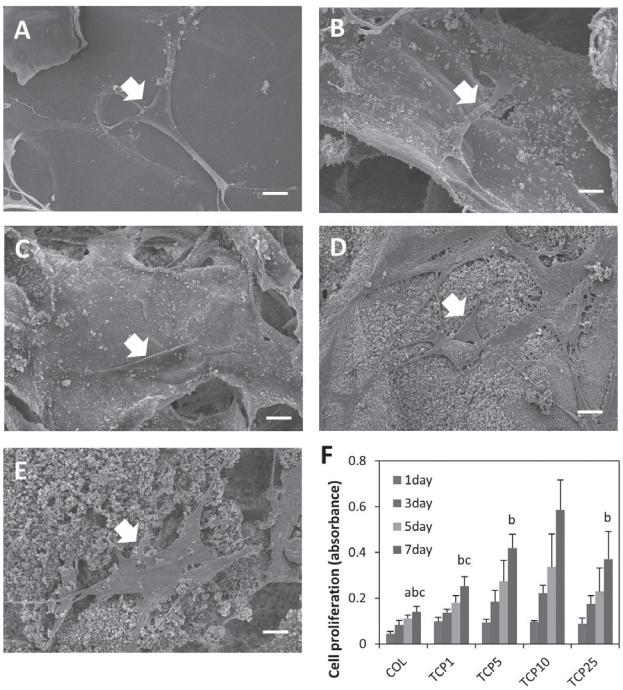

Fig. 5 SEM micrographs of cell morphology on COL (A), TCP1 (B), TCP5 (C), TCP10 (D) and TCP25 (E). Cell spreading on the scaffolds is shown (white arrows). (F) Cell proliferation assay (n=6, mean±SD). Scale bars represent 10 μm (A–E). a, p<0.05 *vs.* TCP25; b, p<0.05 *vs.* TCP10; c, p<0.05 *vs.* TCP5.

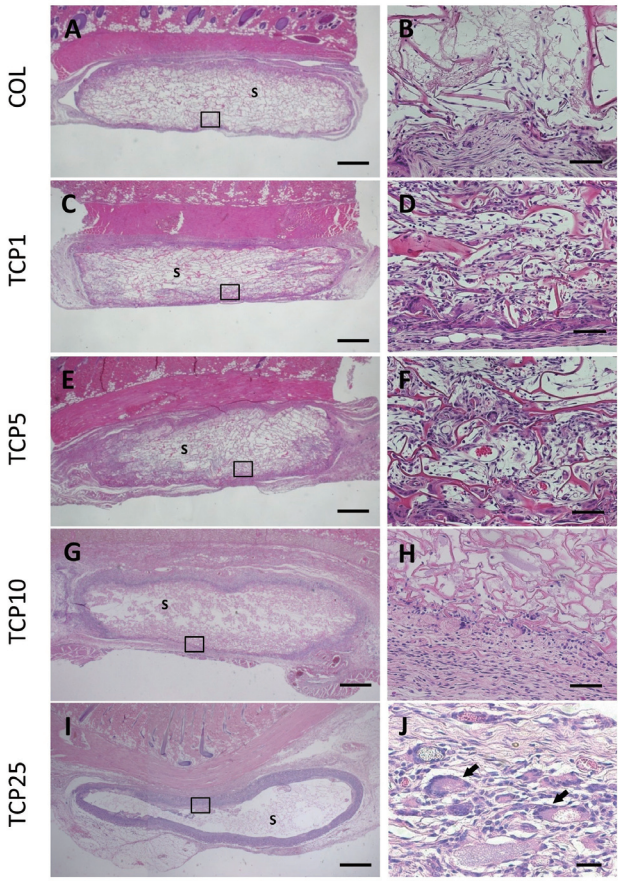

Fig. 6 Histologic findings in rat subcutaneous tissue at 10 days for implanted COL (A), TCP1 (C), TCP5 (E), TCP10 (G), and TCP25 (I).
(B), (D), (F), (H), and (J) respectively represent higher magnifications of the framed areas in (A), (C), (E), (G), and (I). Abbreviations: S denotes scaffold. Scale bars respectively represent 1 mm (A, C, E, G, and I), 50 μm (B, D, F, H), and 20 μm (J). Arrows represent foreign body multinucleate giant cells. Staining: hematoxylin-eosin.

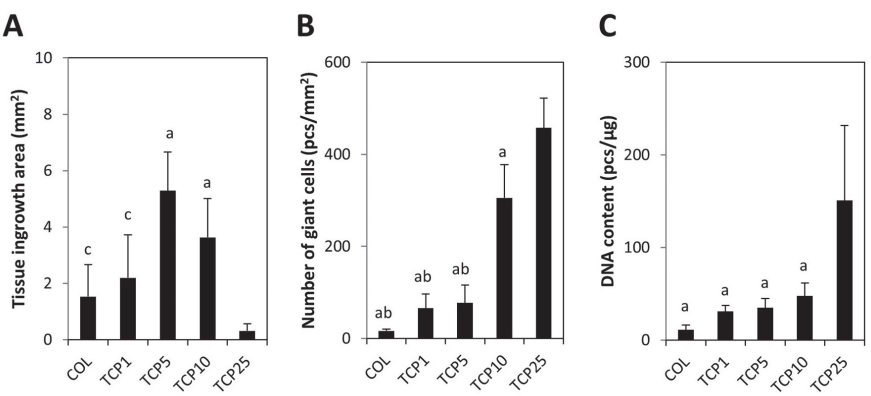

Fig. 7 Measurements of tissue-ingrowth area (A), number of giant cells (B), and DNA content (C) at 10 days for implanted scaffolds (n=6, mean±SD).
a, p<0.05 *vs.* TCP25; b, p<0.05 *vs.* TCP10; c, p<0.05 *vs.* TCP5; d, p<0.05 *vs.* TCP1.

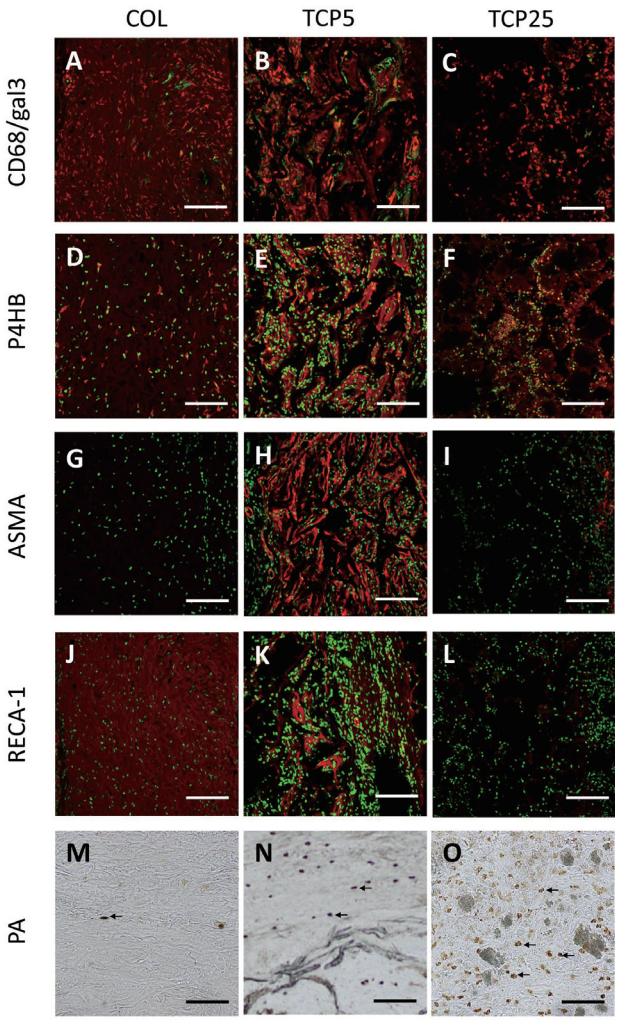

Fig. 8 Immunohistologic staining of CD68 and gal3 (A, B, and C), P4HB (D, E, and F), ASMA (G, H, and I), RECA-1 (J, K, and L), and peroxidase activity (PA) (M, N, and O) in rat subcutaneous tissue at 10 days for implanted COL (A, D, G, J, and M), TCP5 (B, E, H, K, and N), and TCP25 (C, F, I, L, and O).
CD68, P4HB, ASMA and RECA-1 are shown in red, and gal3 and the nucleus of all cells are shown in green. Arrows indicate peroxidase-positive neutrophils. Scale bars respectively represent 100 μm (A–L) and 20 μm (M–O).

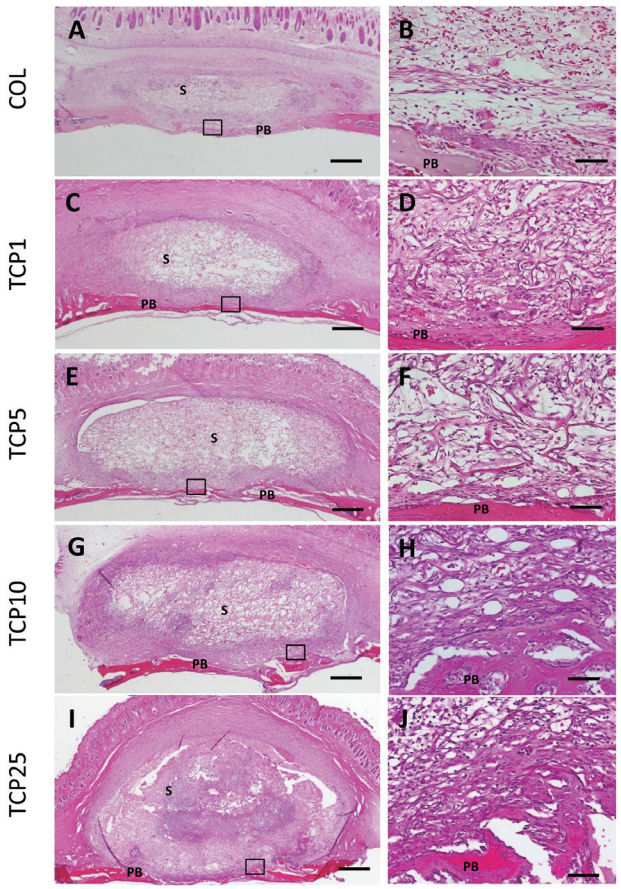

Fig. 9 Histologic findings in rat cranial bone at 10 days for implanted COL (A), TCP1 (C), TCP5 (E), TCP10 (G), and TCP25 (I).
(B), (D), (F), (H), and (J) present higher magnifications of the framed areas in (A), (C), (E), (G), and (I), respectively. Abbreviations: S and PB respectively indicate scaffold and pre-existing bone. Scale bars respectively represent 1 mm (A, C, E, G, I) and 50 μm (B, D, F, H, J). Staining: hematoxylin-eosin.

evidence of existing smooth muscle cells expressing ASMA and endothelial cells expressing RECA-1 in TCP5 (Figs. 8H and K). Therefore, β-TCP nanoparticle application appears to stimulate neovascularization and provide benefits such as oxygen and nutrition supply to the regenerative space for reconstruction of tissues and organs. The cell-ingrowth area in TCP10 and TCP25 was significantly smaller when compared with TCP5 (Fig. 7A). Data regarding foreign body giant cells and DNA content within the implanted scaffolds are presented in Figs. 7B and C. TCP10 and TCP25 exhibited significantly more giant cells and greater DNA content when compared to other scaffolds, although cell and blood vessel infiltration into the central region of these scaffold was rarely demonstrated (Figs. 6G–J, 8F, I, and L). The marginal regions of TCP10 and TCP25 were shown to contain numerous aggregated CD68-positive cells and peroxidase-positive granulocytes (Figs. 8C and O), suggesting that inflammatory cells such as macrophages and neutrophils aggregate on the TCP10 and TCP25 surfaces, absorbing β-TCP nanoparticles by phagocytosis.

Rat bone forming test

At 10 days after implantation on cranial bone, TCP1, TCP5, and TCP10 were able to maintain the regenerative inner space and receive active cell infiltration. In

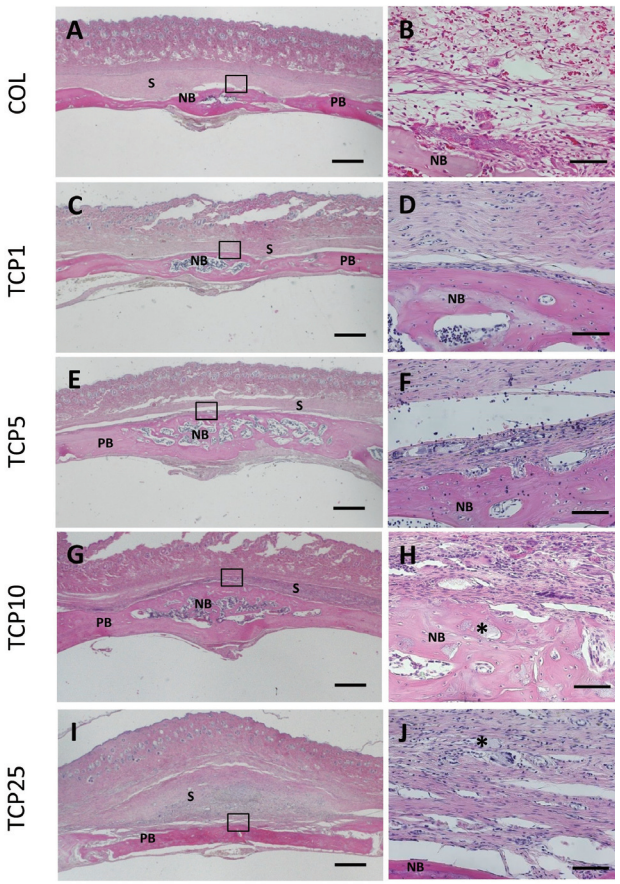

Fig. 10 Histologic findings in rat cranial bone at 35 days for implanted COL (A), TCP1 (C), TCP5 (E), TCP10 (G), and TCP25 (I).
(B), (D), (F), (H), and (J) present higher magnifications of the framed areas in (A), (C), (E), (G), and (I), respectively. Abbreviations: S, PB, and NB respectively denote scaffold, pre-existing bone, and new bone. Stars denote TCP aggregates. Scale bars respectively represent 1 mm (A, C, E, G, I) and 50 μm (B, D, F, H, J). Staining: hematoxylin-eosin.

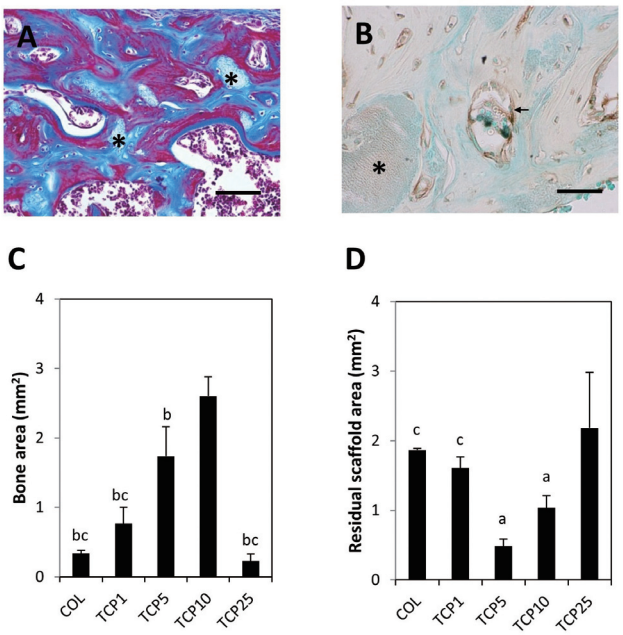

Fig. 11 Histologic findings in rat cranial bone at 35 days for implanted TCP10 (A, B).
Arrows and stars represent osteoblasts and TCP aggregates. Scale bars represent 50 μm (A) and 20 μm (B). Staining: Masson's Trichrome (A) and ALPase (B). Histologic measurement of bone area (C) and residual scaffold area (D) (n=6, mean±SD). a, p<0.05 *vs.* TCP25; b, p<0.05 *vs.* TCP10; c, p<0.05 *vs.* TCP5.

contrast, COL appeared to be physically compressed (Figs. 9A–H). TCP25 consistently induced biomaterial-associated inflammation, such as severe tissue swelling and the infiltration of leukocytes (Figs. 9I and J). In specimens receiving TCP1, TCP5, and TCP10 at 35 days, marked dose-dependent bone augmentation continuous with the pre-existing bone occurred following application of β-TCP nanoparticles (Figs. 10A–H). Newly formed bone frequently included collagen substrate, osteoblastic cells, and micro-aggregated β-TCP nanoparticle residue (Figs. 11A and B). The bone area of TCP5 and TCP10 was, respectively, 5.3- and 7.7-fold greater than that of COL (Fig. 11C). In addition, the amount of residual scaffold of TCP5 and TCP10 was significantly lower when compared with COL (Fig. 11D). Conversely, TCP25 exhibited markedly limited bone augmentation on the cranial bone, irrespective of the application of a high dose of β-TCP (Fig. 10I). Condensed β-TCP nanoparticles were demonstrated in the area of implanted scaffolds, but these particles seemed to have no relationship to bone formation (Fig. 10J). The degree of bone formation of TCP25 was significantly less than that of TCP5 or TCP10 (Fig. 11C).

DISCUSSION

In this study, surface modification with nano-fine structures such as β-TCP nanoparticles resulted in markedly increased bioactivity on 3D scaffolds made of collagen. Particularly, *in vitro* cell proliferation and *in vivo* cell and blood vessel ingrowth effects were strongly up-regulated, which is expected to guide tissue remodeling smoothly. We also found that application of a high dose of β-TCP nanoparticles to the scaffold adversely affected cell and tissue behaviors. Contrary to our expectations, TCP25 suppressed the proliferation of MC3T3-E1 cell in cultures when compared with low-dose application of β-TCP nanoparticles (*i.e.*, TCP10). In addition, histologic analyses revealed that specimens receiving scaffolds with high-dose β-TCP modification,

especially TCP25, exhibited low tissue affinity after implantation in rats, as evidenced by macrophage aggregation and severe inflammation, leading to abnormal healing.

Fabricated scaffolds consisting only of bovine atelocollagen and β-TCP as the artificial substrate are generally recognized as biosafe materials[36,37]. Accordingly, we hypothesized that some physical and chemical properties of the scaffolds nano-modified with β-TCP were associated with the observed adverse biological effects. In SEM observation, TCP25 showed a thick layer of β-TCP nanoparticles that thoroughly coated the collagen scaffold surface. Therefore, the cell attachment apparatus could not stably attach to the base strut of the collagen scaffold, suggesting that the unstable structure used as scaffolding affected cell proliferation. Calcium release test produced evidence that TCP25 released higher levels of calcium ion than the other scaffolds. Maeno *et al.* revealed earlier that osteoblast viability, such as growth and survival rate, was decreased by the application of high concentrations of calcium ions, demonstrating a dose-dependent inverse effect of calcium ions on cell activity[38]. Sugimoto *et al.* reported that high calcium ion concentrations stimulated chemotactic responses in monocytes, associated with macrophage differentiation and inflammatory responses, as well as osteoblastic cell proliferation[39]. These reports are consistent with our results showing that the numbers of CD68-positive cells and giant cells increased in specimens receiving a high dose of β-TCP nanoparticles, demonstrating that calcium ion release from β-TCP scaffolds might play a major role in cellular response and function following scaffold implantation.

Watari *et al.* reported a nanosizing effect when nanomaterial was applied in the body[40]. For instance, the production of superoxide in relation to cellular phagocytosis increased with a subsequent decrease in titanium (Ti) particle size, especially below 10 μm. They also reported that in human neutrophils, Ti particles smaller than 10 μm promoted production of IL-1β and TNF-α, which are related to tissue inflammation. However, these phenomena occurred to a lesser degree for particles smaller than 200 nm. The particle size distribution analyses in the present study showed that β-TCP nanoparticles were approximately 100 nm in diameter. However, SEM images of TCP25 frequently showed aggregation of nanoparticles. The application of high doses of nano-sized β-TCP dispersion created micrometer-sized secondary particles by agglutination, thereby stimulating inflammatory responses and phagocytosis by macrophages. In fact, TCP25 application consistently caused swelling and inflammatory cell infiltration both in rat subcutaneous tissue and cranial bone tests.

Examination of the scaffold physical properties revealed that the compressive strength and collagenase resistance was increased in a dose-dependent manner by the application of β-TCP nanoparticles, suggesting that a thick coating layer consisting of β-TCP nanoparticles and the resulting attractive forces associated with the nanoscale distance between particles enhanced the collagen-based scaffold stability. In bone regenerative therapy, mechanical stiffness of the scaffold can play an important role in maintaining the inner tissue-reconstructive space for osteogenic cells such as osteoblasts[41,42]. Regenerative scaffolds should be designed to provide a highly porous structure for the stimulation of tissue ingrowth. However, higher porosity is generally associated with lower mechanical strength[43,44]. SEM images of TCP5 exhibited evidence of an interconnected porous structure in relation to high porosity, but images of TCP25 showed that the porous space was partly filled with clumps of aggregated TCP nanoparticles. We hypothesized that these results also indicate decreased cellular ingrowth behavior and subsequent bone formation in rats. In fact, numerous giant cells were observed around the aggregated β-TCP granules in the specimens receiving TCP25; therefore, tissue ingrowth might be promoted following severe degradation of β-TCP granules. A regenerative scaffold modified with β-TCP nanoparticles at an optimal dose and exhibiting the excellent porous structure of TCP5 could play an important role in tissue engineering.

The results of bone-forming assessments in rats revealed that bone augmentation was promoted to a considerable degree, compared to COL, by provision of TCP5 or TCP10. However, TCP25 consistently exhibited slight bone formation after implantation, similar to COL-treated histologic specimens. Many previous investigators have reported that β-TCP possesses good osteoconductivity and degradability as a bone graft material when implanted into the bone tissue. They also reported that β-TCP phagocytosis provides calcium ions for osseous induction following osteoblast proliferation[45-47]. As described above, TCP25 strongly induced release of calcium ions, irrespective of macrophage phagocytosis. Therefore, an overdose of calcium ions in the bone-forming field is expected to decrease osteoblastic activity[39,48,49]. In addition, histologic analysis of specimens from TCP25 implantation at 10 days showed severe inflammatory responses, such as swelling. Therefore, high doses of β-TCP nanoparticles negatively affect the biocompatibility of the scaffold for bone tissue engineering. Subsequently, bone augmentation would not be provided. Interestingly, although TCP10 exhibited adverse effects such as prominent macrophage aggregation in subcutaneous tissue, it exhibited positive effects on bone augmentation in cranial bone. Therefore, we presumed that the bioactivity of β-TCP nanoparticles is site specific. Furthermore, β-TCP in combination with several growth factors promoted prominent bone formation as well as cell proliferation and neovascularization[50,51]. Therefore, additional investigations must be conducted to facilitate further development of β-TCP nanoparticle therapy.

CONCLUSION

Dose effects of β-TCP nanoparticles applied to 3D collagen scaffolds were examined *in vitro* and *in vivo*.

Application of β-TCP nanoparticles enhanced the physical properties of the scaffold. TCP5 implantation promoted cell-ingrowth behavior and new blood vessel formation in subcutaneous tissue. Osteoblastic cell proliferation and rat bone augmentation by TCP10 were greater than for any other scaffold. However, TCP25 consistently exhibited adverse biological effects. These results suggest that the application dose of β-TCP nanoparticles affects scaffold biocompatibility and bone conductive ability and suggest that β-TCP nanoparticle therapy using TCP5 and TCP10 shows the greatest potential for use in bone tissue engineering.

ACKNOWLEDGMENTS

The authors would like to thank Olympus Terumo Biomaterials for providing collagen scaffolds and Tomita Pharmaceutical for providing β-TCP. This work was supported by JPSP KAKENHI Grant nos. JP22791916 and JP25463210. The authors report that they have no conflict of interest related to this study.

REFERENCES

1) O'Keefe RJ, Mao J. Bone tissue engineering and regeneration: from discovery to the clinic —an overview. Tissue Eng Part B Rev 2011; 17: 389-392.
2) Stoppato M, Stevens HY, Carletti E, Migliaresi C, Motta A, Guldberg RE. Influence of scaffold properties on the inter-relationship between human bone marrow derived stromal cells and endothelial cells in pro-osteogenic conditions. Acta Biomater 2015; 25: 16-23.
3) Zhang R, Lee P, Lui VC, Chen Y, Liu X, Lok CN, To M, Yeung KW, Wong KK. Silver nanoparticles promote osteogenesis of mesenchymal stem cells and improve bone fracture healing in osteogenesis mechanism mouse model. Nanomedicine 2015; 11: 1949-1959.
4) Fawzy El-Sayed KM, Mekhemar MK, Beck-Broichsitter BE, Bähr T, Hegab M, Receveur J, Heneweer C, Becker ST, Wiltfang J, Dörfer CE. Periodontal regeneration employing gingival margin-derived stem/progenitor cells in conjunction with IL-1ra-hydrogel synthetic extracellular matrix. J Clin Periodontol 2015; 42: 448-457.
5) Chang CC, Tsai YH, Liu Y, Lin SY, Liang YC. Calcium-containing crystals enhance receptor activator of nuclear factor κB ligand/macrophage colony-stimulating factor-mediated osteoclastogenesis via extracellular-signal-regulated kinase and p38 pathways. Rheumatology (Oxford) 2015; 54: 1913-1922.
6) Carreira AC, Zambuzzi WF, Rossi MC, Filho RA, Sogayar MC, Granjeiro JM. Bone morphogenetic proteins: Promising molecules for bone healing, bioengineering, and regenerative medicine. Vitam Horm 2015; 99: 293-322.
7) Tian J, Qi W, Zhang Y, Glogauer M, Wang Y, Lai Z, Jiang H. Bioaggregate inhibits osteoclast differentiation, fusion, and bone resorption in vitro. J Endod 2015; 41: 1500-1506.
8) Carrel JP, Wiskott A, Moussa M, Rieder P, Scherrer S, Durual S. A 3D printed TCP/HA structure as a new osteoconductive scaffold for vertical bone augmentation. Clin Oral Implants Res 2016; 27: 55-62.
9) Yoshida T, Miyaji H, Otani K, Inoue K, Nakane K, Nishimura H, Ibara A, Shimada A, Ogawa K, Nishida E, Sugaya T, Sun L, Fugetsu B, Kawanami M. Bone augmentation using a highly porous PLGA/b-TCP scaffold containing fibroblast growth factor-2. J Periodontal Res 2015; 50: 265-273.
10) Kosen Y, Miyaji Y, Kato A, Sugaya T, Kawanami M. Application of collagen hydrogel/sponge scaffold facilitates periodontal wound healing in class II furcation defects in beagle dogs. J Periodontal Res 2012; 47: 626-634.
11) Niu CC, Lin SS, Chen WJ, Liu SJ, Chen LH, Yang CY, Wang CJ, Yuan LJ, Chen PH, Cheng HY. Benefits of biphasic calcium phosphate hybrid scaffold-driven osteogenic differentiation of mesenchymal stem cells through upregulated leptin receptor expression. J Orthop Surg Res 2015; 10: 1-10.
12) Yu N, Bronckers AL, Oortgiesen DA, Yan X, Jansen JA, Yang F, Walboomers XF. Periodontal cell implantation contributes to the regeneration of the periodontium in an indirect way. Tissue Eng Part A 2015; 21: 166-173.
13) Rasperini G, Pilipchuk SP, Flanagan CL, Park CH, Pagni G, Hollister SJ, Giannobile WV. 3D-printed bioresorbable scaffold for periodontal repair. J Dent Res 2015; 94: 153-157.
14) Wu PH, Chung HY, Wang JH, Shih JC, Kuo MY, Chang PC, Huang Y, Wang PC, Chang CC. Amniotic membrane and adipose-derived stem cell co-culture system enhances bone regeneration in a rat periodontal defect model. J Formos Med Assoc 2016; 115: 186-194.
15) Requicha JF, Viegas CA, Muñoz F, Azevedo JM, Leonor IB, Reis RL, Gomes ME. A tissue engineering approach for periodontal regeneration based on a biodegradable double-layer scaffold and adipose-derived stem cells. Tissue Eng Part A 2014; 20: 2483-2492.
16) Dimitriou R, Jones E, McGonagle D, Giannoudis PV. Bone regeneration: current concepts and future directions. BMC Med 2011; 9: 66.
17) Fitzgerald KA, Guo J, Tierney EG, Curtin CM, Malhotra M, Darcy R, O'Brien FJ, O'Driscoll CM. The use of collagen-based scaffolds to simulate prostate cancer bone metastases with potential for evaluating delivery of nanoparticulate gene therapeutics. Biomaterials 2015; 66: 53-66.
18) Aloy-Prósper A, Peñarrocha-Oltra D, Peñarrocha-Diago M, Peñarrocha-Diago M. Dental implants with versus without peri-implant bone defects treated with guided bone regeneration. Clin Exp Dent 2015; 7: 361-368.
19) Park SH, Wang HL. Management of localized buccal dehiscence defect with allografts and acellular dermal matrix. Int J Periodontics Restorative Dent 2006; 26: 589-595.
20) Min Z, Shichang Z, Chen X, Yufang Z, Changqing Z. 3D-printed dimethyloxallyl glycine delivery scaffolds to improve angiogenesis and osteogenesis. Biomater Sci 2015; 3: 1236-1244.
21) Zheng H, Bai Y, Shih MS, Hoffmann C, Peters F, Waldner C, Hübner WD. Effect of a β-TCP collagen composite bone substitute on healing of drilled bone voids in the distal femoral condyle of rabbits. J Biomed Mater Res B Appl Biomater 2014; 102: 376-383.
22) Yuan H, van Blitterswijk CA, de Groot K, de Bruijn JD. Cross-species comparison of ectopic bone formation in biphasic calcium phosphate (BCP) and hydroxyapatite (HA) scaffolds. Tissue Eng 2006; 12: 1607-1615.
23) Okada S, Nagai A, Oaki Y, Komotori J, Imai H. Control of cellular activity of fibroblasts on size-tuned fibrous hydroxyapatite nanocrystals. Acta Biomater 2011; 7: 1290-1297.
24) Kankilic B, Köse S, Korkusuz P, Timuçin M, Korkusuz F. Mesenchymal stem cells and nano-bioceramics for bone regeneration. Curr Stem Cell Res Ther 2016; 11: 487-493.
25) Kim SS, Sun Park M, Jeon O, Yong Choi C, Kim BS. Poly(lactide-co-glycolide)/hydroxyapatite composite scaffolds for bone tissue engineering. Biomaterials 2006; 27: 1399-1409.
26) Casarrubios L, Matesanz MC, Sánchez-Salcedo S, Arcos D, Vallet-Regí M, Portolés MT. Nanocrystallinity effects on osteoblast and osteoclast response to silicon substituted hydroxyapatite. J Colloid Interface Sci 2016; 482: 112-120.
27) Ibara A, Miyaji H, Fugetsu B, Nishida E, Takita H,

Tanaka S, Sugaya T, Kawanami M. Osteoconductivity and biodegradability of collagen scaffold coated with nano-β-TCP and fibroblast growth factor 2. J Nanomaterials 2013; ID639502: 1-11
28) Ogawa K, Miyaji H, Kato A, Kosen Y, Momose T, Yoshida T, Nishida E, Miyata S, Murakami S, Takita H, Fugetsu B, Sugaya T, Kawanami M. Periodontal tissue engineering by nano beta-TCP scaffold and FGF-2 in 1-wall inrabony defects of dogs. J Periodontal Res 2016; 51: 758-767.
29) Huang J, Best SM, Bonfield W, Brooks RA, Rushton N, Jayasinghe SN, Edirisinghe MJ. In vitro assessment of the biological response to nano-sized hydroxyapatite. J Mater Sci Mater Med 2004; 15: 441-445.
30) Nishida E, Miyaji H, Takita H, Kanayama I, Tsuji M, Akasaka T, Sugaya T, Sakagami R, Kawanami M. Graphene oxide coating facilitates the bioactivity of scaffold material for tissue engineering. Jpn J Appl Phys 2014; 53: 1-7.
31) Schrand AM, Huang H, Carlson C, Schlager JJ, Omacr Sawa E, Hussain SM, Dai L. Are diamond nanoparticles cytotoxic? J Phys Chem B 2007; 111: 2-7.
32) Meenambal R, Poojar P, Geethanath S, Kannan S. Substitutional limit of gadolinium in β-tricalcium phosphate and its magnetic resonance imaging characteristics. J Biomed Mater Res B Appl Biomater 2016; in press.
33) Gao C, Wei P, Feng P, Xiao T, Shuai C, Peng S. Nano SiO2 and MgO Improve the Properties of Porous β-TCP Scaffolds via Advanced Manufacturing Technology. Int J Mol Sci 2015; 16: 6818-6830.
34) Padmanabhan SK, Salvatore L, Gervaso F, Catalano M, Taurino A, Sannino A, Licciulli A. Synthesis and characterization of collagen scaffolds reinforced by eggshell derived hydroxyapatite for tissue engineering. J Nanosci Nanotechnol 2015; 15: 504-509.
35) Oda K, Amaya Y, Fukushi-Irié M, Kinameri Y, Ohsuye K, Kubota I, Fujimura S, Kobayashi J. A general method for rapid purification of soluble versions of glycosylphosphatidylinositol-anchored proteins expressed in insect cells: an application for human tissue-nonspecific alkaline phosphatase. J Biochem 1999; 126: 694-699.
36) Deng Y, Zhou H, Yan C, Wang Y, Xiao C, Gu P, Fan X. In vitro osteogenic induction of bone marrow stromal cells with encapsulated gene-modified bone marrow stromal cells and in vivo implantation for orbital bone repair. Tissue Eng Part A 2014; 20: 2019-2029.
37) Guan J, Zhang J, Li H, Zhu Z, Guo S, Niu X, Wang Y, Zhang C. Human urine derived stem cells in combination with β-TCP can be applied for bone regeneration. PLoS One 2015; 10: 1-16.
38) Maeno S, Niki Y, Matsumoto H, Morioka H, Yatabe T, Funayama A, Toyama Y, Taguchi T, Tanaka J. The effect of calcium ion concentration on osteoblast viability, proliferation and differentiation in monolayer and 3D culture. Biomaterials 2005; 26: 4847-4855.
39) Sugimoto T, Kanatani M, Kano J, Kaji H, Tsukamoto T, Yamaguchi T, Fukase M, Chihara K. Effects of high calcium concentration on the functions and interactions of osteoblastic cells and monocytes and on the formation of osteoclast-like cells. J Bone Miner Res 1993; 8: 1445-1452.
40) Watari F, Takashi N, Yokoyama A, Uo M, Akasaka T, Sato Y, Abe S, Totsuka Y, Tohji K. Material nanosizing effect on living organisms: non-specific, biointeractive, physical size effects. J R Soc Interface 2009; 6: 371-388.
41) Chuenjitkuntaworn B, Osathanon T, Nowwarote N, Supaphol P, Pavasant P. The efficacy of polycaprolactone/hydroxyapatite scaffold in combination with mesenchymal stem cells for bone tissue engineering. J Biomed Mater Res A 2015; 104: 264-271.
42) Kerativitayanan P, Gaharwar AK. Elastomeric and mechanically stiff nanocomposites from poly(glycerol sebacate) and bioactive nanosilicates. Acta Biomater 2015; 26: 34-44.
43) Bose S, Darsell J, Kintner M, Hosick H, Bandyopadhyay A. Pore size and pore volume effects on alumina and TCP ceramic scaffolds. Mater Sci Eng C 2003; 23: 479-485.
44) Kasten P, Beyen I, Niemeyer P, Luginbuhl R, Bohner M, Richter W. Porosity and pore size of β-tricalcium phosphate scaffold can influence protein production and osteogenic differentiation of human mesenchymal stem cells: an in vitro and in vivo study. Acta Biomater 2008; 4: 1904-1915.
45) Saito M, Shimizu H, Beppu M, Takagi M. The role of beta-tricalcium phosphate in vascularized periosteum. J Orthop Sci 2000; 5: 275-282.
46) Koepp HE, Schorlemmer S, Kessler S, Brenner RE, Claes L, Günther KP, Ignatius AA. Biocompatibility and osseointegration of β-TCP: Histomorphological and biomechanical studies in a weight-bearing sheep model. J Biomed Mater Res Part B 2004; 70: 209-217.
47) Kunert-Keil C, Scholz F, Gedrange T, Gredes T. Comparative study of biphasic calcium phosphate with beta-tricalcium phosphate in rat cranial defects —A molecular-biological and histological study. Ann Anat 2015; 199: 79-84.
48) Adams CS, Mansfield K, Perlot RL, Shapiro IM: Matrix regulation of skeletal cell apoptosis. Role of calcium and phosphate ions. J Biol Chem 2001; 276: 20316-20322.
49) Meleti Z, Shapiro IM, Adams CS. Inorganic phosphate induces apoptosis of osteoblast-like cells in culture. Bone 2000; 27: 359-366.
50) Zhang X, Meng S, Huang Y, Xu M, He Y, Lin H, Han J, Chai Y, Wei Y, Deng X. Electrospun gelatin/β-TCP composite nanofibers enhance osteogenic differentiation of BMSCs and in vivo bone formation by activating Ca (2+) —sensing receptor signaling. Stem Cells Int 2015; 2015: 1-13.
51) Chen Y, Wang J, Zhu XD, Tang ZR, Yang X, Tan YF, Fan YJ, Zhang XD. Enhanced effect of β-tricalcium phosphate phase on neovascularization of porous calcium phosphate ceramics: in vitro and in vivo evidence. Acta Biomater 2015; 11: 435-448.